Journal of Applied Physics

High performance blue-emitting organic light-emitting diodes from thermally activated delayed fluorescence: A guest/host ratio study

Cite as: J. Appl. Phys. **124**, 055501 (2018); https://doi.org/10.1063/1.5041447
Submitted: 24 May 2018 . Accepted: 18 July 2018 . Published Online: 07 August 2018

Xiaoqing Zhang, Canek Fuentes-Hernandez, Yadong Zhang, Matthew W. Cooper, Stephen Barlow, Seth R. Marder, and Bernard Kippelen

High performance blue-emitting organic light-emitting diodes from thermally activated delayed fluorescence: A guest/host ratio study

Xiaoqing Zhang,[1] Canek Fuentes-Hernandez,[1] Yadong Zhang,[2] Matthew W. Cooper,[2] Stephen Barlow,[2] Seth R. Marder,[2] and Bernard Kippelen[1,a)]
[1]*Center for Organic Photonics and Electronics (COPE), School of Electrical and Computer Engineering, Georgia Institute of Technology, Atlanta, Georgia 30332, USA*
[2]*Center for Organic Photonics and Electronics (COPE), School of Chemistry and Biochemistry, Georgia Institute of Technology, Atlanta, Georgia 30332, USA*

(Received 24 May 2018; accepted 18 July 2018; published online 7 August 2018)

Emitters displaying thermally activated delayed fluorescence (TADF) can lead to highly efficient organic light-emitting diodes (OLEDs). Such emitters are usually incorporated into the emissive layer (EML) at a relatively low concentration (<20 wt. %) with respect to a host material, a guest-host approach inherited from conventional fluorescent or phosphorescent OLEDs. Here, detailed studies on OLEDs, in which the concentration of oBFCzTrz (a blue-emitter displaying TADF) in a DPEPO host was varied from 8 to 100 wt. %, reveals that oBFCzTrz displays ambipolar transport and limited fluorescence-quenching due to aggregation. For instance, a neat film of oBFCzTrz maintains a photoluminescence quantum yield of 82%. We demonstrate that OLEDs with an EML having an oBFCzTrz concentration of 50 wt. % in DPEPO yield a maximum external quantum efficiency (EQE) of 25.5% with an EQE roll-off of 10% in the range from 10 to 1000 cd/m^2 and Commission Internationale de l'Eclairage color coordinates of (0.20, 0.44). OLEDs with smaller or larger oBFCzTrz concentrations display smaller maximum EQE values. OLEDs with a neat oBFCzTrz EML display a maximum EQE of 14.0%. Time-resolved electroluminescent decay studies, and analysis using a simple model, reveal significant differences in transport, trapping, and recombination in these devices. *Published by AIP Publishing.* https://doi.org/10.1063/1.5041447

I. INTRODUCTION

Organic light-emitting diodes (OLEDs) are attractive for next-generation displays and solid-state lighting. In recent years, fluorescent organic molecules displaying thermally activated delayed fluorescence (TADF) have enabled emissive layers (EMLs) that lead to devices with an internal quantum efficiency (IQE) of ca. 100%. Previously, similar values could only be achieved using phosphorescent emitters.[1–3] A TADF emitter can lead to devices with such high IQE values if its singlet-triplet energy separation (ΔE_{ST}) is sufficiently small to facilitate reverse intersystem crossing (RISC) from the triplet excited states to the singlet excited states at a rate that is substantially faster than the decay rate of the triplet excited states.[4] Maximum external quantum efficiency (EQE) values displayed by OLEDs with TADF-based emissive layers have been reported to be 37% for a sky-blue device,[5] over 30% for a green device,[6] and nearly 30% for an orange-red device.[7]

Although RISC can lead to efficient triplet harvesting, it also results in excited-state lifetimes that are comparable to those found in phosphorescent emitters, the delayed portion of the fluorescence typically exhibiting decay constants in the range of tens to hundreds of microseconds. Long-lived excited states in TADF or phosphorescent emitters are known to play an important role in causing significant EQE roll-off as the luminance of an OLED is increased above values of ca. 1000 cd/m^2.[8] Under these operational conditions, a large current density leads to a large density of long-lived triplet excitons and an increased probability of emission quenching through triplet-triplet annihilation (TTA), triplet-polaron annihilation (TPA), and other non-radiative recombination processes.[9] Moreover, in blue-emitting compounds, the energy dissipated by some of these exciton-quenching reactions can be sufficiently large to initiate bond-cleavage and produce irreversible damage to the EML, consequently severely reducing the lifetime of the OLED. While the EQE roll-off and device lifetime can be influenced by many other mechanisms, achieving OLEDs that display low EQE roll-off values is an important step towards improving the performance and lifetime of blue-emitting OLEDs.[10]

Recently, TADF emitters using donor moieties, such as acridane or carbazole derivatives, and acceptors, such as triazine or diphenylsulfone, have resulted in blue-emitting TADF molecules with estimated ΔE_{ST} values close to zero and delayed fluorescence lifetimes <6 μs (SpiroAC-TRZ,[5] PIC-TRZ2,[11] DMAC-DPS,[12] oBFCzTrz,[15] and DMAC-TRZ[16]). OLEDs based on these emitters have been shown to display EQE roll-off that can be quantified by a 20% and 50% reduction in EQE from its maximum value at luminance levels of 1000 and 10 000 cd/m^2, respectively.[5] In many devices, TADF emitters are sparsely embedded in a host matrix at low doping concentration (<20 wt. %) to prevent aggregation-quenching,[13–15] an EML-design paradigm inherited from fluorescent and phosphorescent OLEDs. However,

a)Author to whom correspondence should be addressed: kippelen@ece.gatech.edu

an increasing number of reports suggest that OLEDs in which the emissive layer are composed exclusively of the TADF emitter can display EQE values up to ca. 20%, and negligible EQE roll-off.[12,16–18] These intriguing results suggest that compounds displaying TADF can display ambipolar transport and limited aggregation-caused fluorescence quenching, challenging our current understanding of concentration quenching mechanisms in OLEDs.[25] Indeed, recent reports[19,20] suggested that the mechanism of fluorescence-quenching in TADF emitters with D-A (Donor-Acceptor) electronic structures is different from that observed in systems comprising conventional fluorescent and phosphorescent emitters, typically involving Förster energy-transfer processes. In contrast, when TADF emitters interact, short-range Dexter energy transfer dominates the concentration quenching, and consequently, bulky TADF molecules with insulating substituents may suppress these intermolecular electron-exchange interactions and thus concentration quenching.

In this work, we report on systematic studies in OLEDs where the concentration of the blue-emitting compound oBFCzTrz (which exhibits TADF due to a ΔE_{ST} of ca. zero) is varied from 8 to 100 wt. % in the widely used host DPEPO. We find that maximum EQE values of 25.5%, with low EQE roll-off values of 10% at 1000 cd/m^2 and 36% at 10 000 cd/m^2, are achieved in OLEDs having an EML comprising 50 wt. % of oBFCzTrz in DPEPO. As reported by Lee *et al.*,[15] we find that OLEDs with an EMLs comprising 20 wt. % of oBFCzTrz doped in DPEPO can reach EQE values over 20%. In contrast, Lee *et al.*[15] reported only results on devices with oBFCzTrz concentrations in the range of 5–30 wt. %. Here, we find that devices with concentrations of oBFCzTrz larger than 30 wt. % continue to display high EQE and low EQE roll-off values. For instance, host-free devices using only an oBFCzTrz neat film as EML yield maximum EQE values of 14.0% at 255 cd/m^2, 13.7% at 1000 cd/m^2, and 9.2% at 10 000 cd/m^2. We also report on the electrical characteristics of hole- and electron-only devices, the results of time-resolved electroluminescent (EL) decay studies, and on an analysis using a simple model that reveals significant differences in the charge injection, transport, trapping, and recombination in these devices.

II. RESULTS AND DISCUSSION

The OLED geometry and chemical structure of the organic molecules used in this study are shown in Fig. 1. The emissive layer comprises the TADF-emitter oBFCzTrz doped at concentrations of 8, 20, 38, 50, 64, 80, and 100 (neat film) wt. % into a DPEPO host. From here on, we will refer to these devices by the label DX, where the letter D refers to device and X refers to the oBFCzTrz weight percentage in the EML.

Figure 2(a) shows the electroluminescent (EL) spectra of all devices when biased at 5 V. Clear changes of the EL spectra are observed when the concentration of oBFCzTrz increases from 8 wt. % to 20 wt. %. For devices with a larger oBFCzTrz concentration, changes in the EL spectral are negligible. Figure 2(a) also shows the calculated Commission Internationale de l'Eclairage (CIE) color coordinates derived from the EL spectra, indicating that the emission color changes from blue in D8, as reported by Lee *et al.*,[15] to sky-blue in D20 devices. A Gaussian decomposition of the EL spectra of D8 and D38, as shown in Fig. 2(b), reveals four peaks centered at 462, 488, 508, and 531 nm, labeled from 1 to 4, respectively. In D38, the amplitude of peak 1 (at 462 nm) is significantly smaller than that in D8. At the same time, the amplitude of peak 4 (at 531 nm) in D38 is significantly larger than the corresponding one in D8. We believe that these changes may result from molecular aggregation as the concentration of oBFCzTrz is increased from 8 wt. % to 38 wt. %. Emissive layers fabricated on quartz and having oBFCzTrz concentrations of 50 and 100 wt. % also display red shifted photoluminescence (PL) spectra (as shown in Fig. S1 of the supplementary material) and decreased photoluminescence quantum yields (PLQYs) (90% and 82%), respectively, relative to that of an 8 wt. % layer (PLQY = 100%) (see Table S1). Despite these apparent aggregation effects, as we will describe next, there is a range of oBFCzTrz

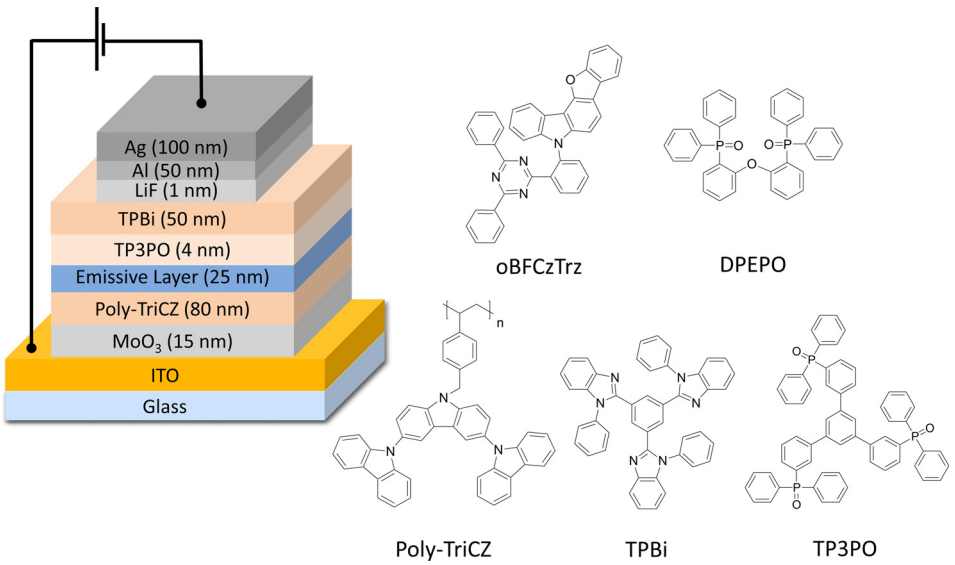

FIG. 1. Device geometry and chemical structures of oBFCzTrz (emitter), DPEPO (host), Poly-TriCZ (hole transporting layer), TPBi and TP3PO (electron transporting layers).

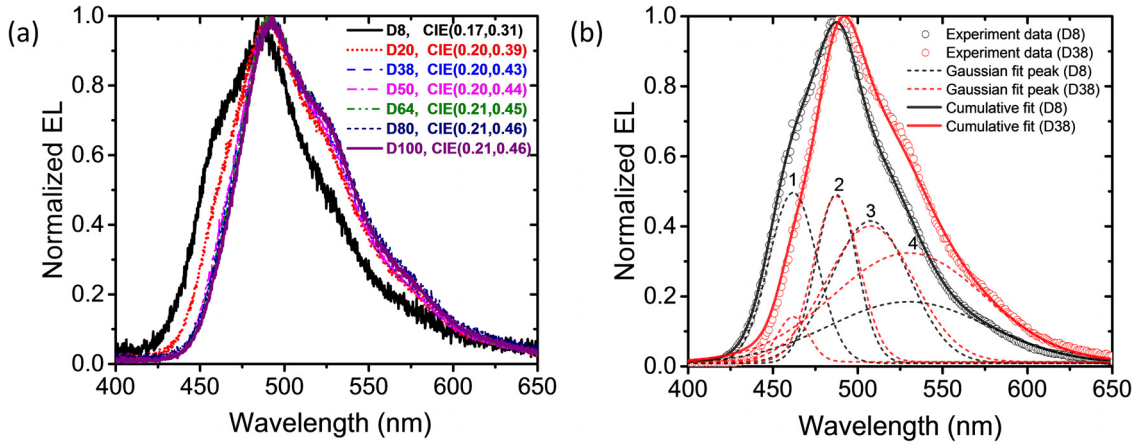

FIG. 2. (a) Normalized EL spectrum of D8, D20, D38, D50, D64, D80, and D100 and their CIE coordinates, respectively; (b) Gaussian peak decomposition of EL spectra of D8 and D38.

concentrations over which the device performance does not seem to be greatly affected.

The *J-V* characteristics of all devices are shown in Fig. 3(a). These data reveal that all devices behave like diodes and exhibit good rectification and comparable current density values, with exception of D8 and D100, which display lower *J* values and larger turn-on voltage. This behavior is also observed in the luminance (*L*) vs. voltage (*V*) characteristics, as shown in Fig. 3(b). Devices D20 to D80 display a turn-on voltage [V_{on}, defined as the voltage needed for $L(V_{on}) = 10\,\mathrm{cd/m^2}$] of ca. 3.4 V, while D8 and D100 display a larger V_{on} of 4.6 V and 4.2 V, respectively. EQE (*L*) values in all devices were normalized by $\mathrm{EQE_{10}} \equiv \mathrm{EQE}\ (10\,\mathrm{cd/m^2})$ to facilitate the comparison of the EQE roll-off characteristics. Figure 3(c) displays the normalized EQE vs. *L* characteristics in all devices and Table I summarizes the performance parameters measured in all devices. The data in Fig. 3(c) show that $\mathrm{EQE_{10}}$ goes from a value of 20.3% in D8

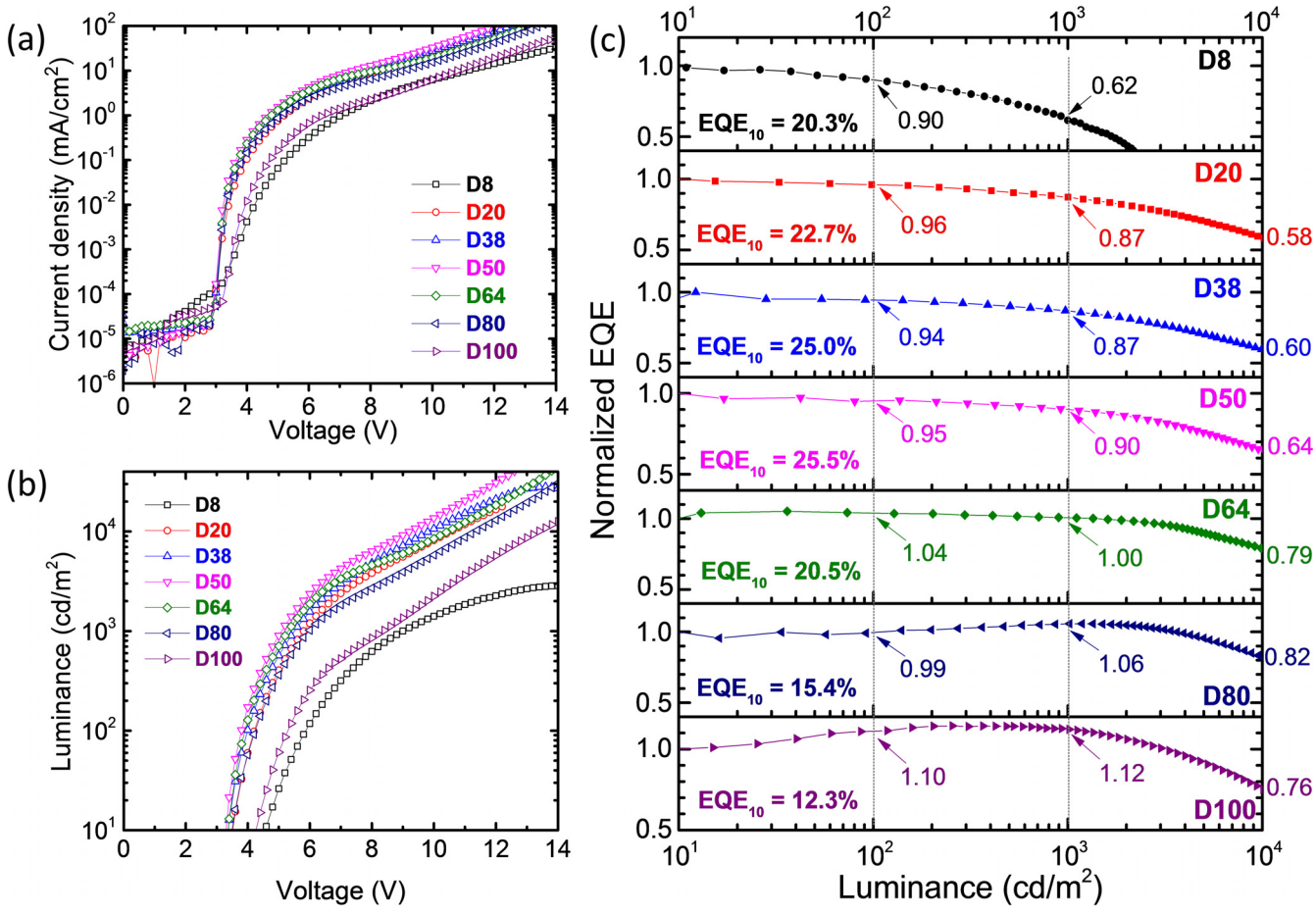

FIG. 3. (a) *J-V* curves; (b) *L-V* curves; and (c) EQE roll-off of D8 to D100, normalized by their $\mathrm{EQE_{10}}$, respectively. The $\mathrm{EQE_{10}}$ value, and the EQE roll-off at 100 cd/m^2, 1000 cd/m^2, and 10 000 cd/m^2 of each device are noted.

TABLE I. Performance characterization of OLEDs with emissive layers doped with various concentrations of oBFCzTrz. (η_c: current efficacy, η_P: power efficacy).

Device name	Emissive layer (Doping concentration, wt. %)	EQE(%) at 10/100/1000/10 000 cd/m^2, EQE_{max}	V_{on} (V) at 10 cd/m^2	η_c(cd/A) at 1000 cd/m^2	η_P(lm/W) at 1000 cd/m^2	CIE (x, y) at 5 V
D8	DPEPO: oBFCzTrz (8%)	20.3/18.5/12.6/ –, 20.3	4.6	25.5	8.9	(0.17, 0.31)
D20	DPEPO: oBFCzTrz (20%)	22.7/21.8/19.8/13.5, 22.7	3.5	51.2	27.8	(0.20, 0.39)
D38	DPEPO: oBFCzTrz (38%)	25.0/24.5/22.4/15.5, 25.0	3.3	54.3	30.5	(0.20, 0.43)
D50	DPEPO: oBFCzTrz (50%)	25.5/24.2/22.8/16.4, 25.5	3.3	58.2	35.0	(0.20, 0.44)
D64	DPEPO: oBFCzTrz (64%)	20.5/21.3/20.6/16.2, 21.3	3.4	53.6	31.7	(0.21, 0.45)
D80	DPEPO: oBFCzTrz (80%)	15.4/15.3/16.3/12.7, 16.3	3.4	42.8	22.5	(0.21, 0.46)
D100	oBFCzTrz (100%)	12.3/13.6/13.7/9.2, 14.0	4.2	37.9	14.2	(0.21, 0.46)

to a maximum of 25.5% in D50, and down to 12.3% in D100. We note that the changes of EQE measured in devices with various concentrations of the oBFCzTrz emitter do not correlate with the changes in PLQY measured in solid films with similar composition (see Table S1). For instance, device D50 shows increased maximum EQE compared to D8, while the PLQY shows an opposite trend. This illustrates that changes in charge balance due to variations in charge injection and charge mobility in these devices in which the emissive layer has different compositions also play an important role.

Before analyzing differences in charge transport between devices, it is worth noting that Fig. 3(c) also shows that generally, as the concentration of oBFCzTrz is increased, devices display a decreasing EQE roll-off. For instance, at 1000 cd/m^2, the EQE roll-off for D8 is 37.9% (i.e., $EQE_{10} = 20.3\%$ goes to $EQE_{1000} = 12.6\%$), while for D64 the EQE roll-off is ca. zero (i.e., $EQE_{10} = 20.5\%$, $EQE_{1000} = 20.6\%$). Interestingly, for D80 and D100, the EQE_{1000} is in fact larger than EQE_{10}; in D100, EQE_{1000} is 11.4% larger than EQE_{10}. For D100, we have found this behavior to be dependent on the thickness of the EML as shown in Fig. S2 of the supplementary material.

The large EQE observed in devices with oBFCzTrz concentrations larger than 50 wt. % strongly suggests that oBFCzTrz has good ambipolar transport, and that hole and electron injection into the EML is reasonably well balanced. Figure 4 shows a comparison of the current density measured in hole-only and electron-only devices for pristine DPEPO and oBFCzTrz. This comparison reveals that, in contrast to DPEPO devices, where the electron-current density is significantly larger than the hole-current density, in devices having a pristine layer of oBFCzTrz the electron and hole-current density are indeed better matched. Although it is not possible to infer energy-level alignment in a device from electrochemical estimations of ionization energies (IEs) and electron affinities (EAs) on isolated molecules, typically carried out in solution rather than in solid-state, solution-based values reported in the literature may offer some initial clue to the differences in hole and electron transport observed in single carrier devices. Based on literature values, DPEPO is expected to have a very wide transport bandgap (ca. 4.2 eV),[15] larger than that of Poly-TriCZ (ca. 3.2 eV)[21] and of TP3PO (ca. 4.0 eV)[22] and TPBi (ca. 3.5 eV).[23] As shown in Fig. S3 of the supplementary material and discussed in the supplementary material, Fermi-level alignment between the different intrinsic semiconductor layers in the device (i.e., after the device is fabricated) could produce a larger energy

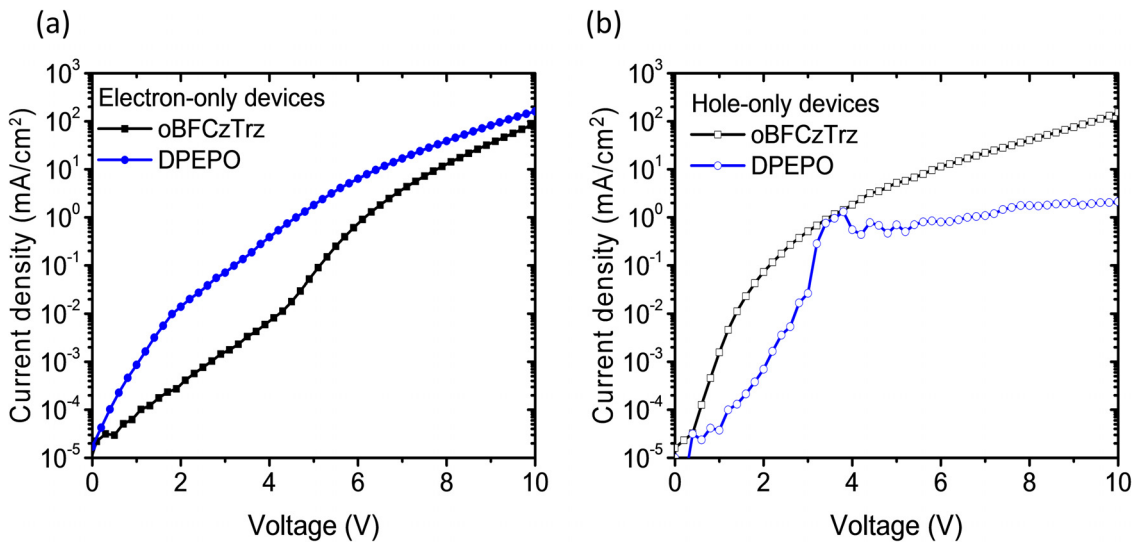

FIG. 4. *J-V* curves of electron-only and hole-only devices employing pristine DPEPO and oBFCzTrz films. (a) Electron-only devices with structure of glass/PEDOT:PSS/Al (50 nm)/LiF (2.5 nm)/TPBi (30 nm)/DPEPO or oBFCzTrz (25 nm)/TP3PO(4 nm)/TPBi (50 nm)/LiF (1 nm)/Al (50 nm)/Ag (100 nm). (b) Hole-only devices with the structure of glass/ITO/MoO_3(15 nm)/Poly-TriCZ(80 nm)/DPEPO or oBFCzTrz (25 nm)/α-NPD(30 nm)/MoO_3(15 nm)/Au (20 nm)/Ag (100 nm).

barrier for hole-injection from Poly-TriCZ (ca. 0.5 eV) than for electron-injection (ca. 0.1 eV from TP3PO and ca. 0.25 eV from TPBi to TP3PO, if electrons are indeed injected into TP3PO instead of tunneling through this layer). Consequently, it is not surprising that a large imbalance between the hole- and the electron-current density is observed in DPEPO devices. We note also that the shape of the current-voltage characteristic of hole-only devices with DPEPO is unusual and deviates from that of the other curves. However, multiple devices were tested and they yielded consistently curves with similar shapes. We attribute this behavior to the poor injection of holes dues to the large barrier for hole-injection at the Poly-TriCZ/DPEPO interface. In contrast, using a similar analysis on oBFCzTrz devices reveals that, in principle, no energy barriers for electron- and hole-injection should be expected since the transport bandgap of oBFCzTrz (ca. 2.7 eV) is significantly smaller than that of Poly-TriCZ, TP3PO, and TPBi.

In an effort to further investigate differences in charge transport, recombination, and electroluminescence between devices having different concentrations of oBFCzTrz, we conducted time-resolved EL measurements on devices D8, D50, and D100 by applying a square-shaped voltage pulse. For devices D50 and D100, voltages were selected to achieve 100 cd/m^2, 500 cd/m^2, 1000 cd/m^2, and 10 000 cd/m^2. For devices D8, voltages were selected to achieve 100 cd/m^2, 500 cd/m^2, and 1000 cd/m^2 since these devices did not reach a luminance of 10 000 cd/m^2 in the voltage range of 0–14 V as shown in Fig. 3(b). The transient EL signal was recorded with an oscilloscope and normalized to the steady-state EL amplitude, as shown in Fig. S4 of the supplementary material. Here $t = 0$ μs corresponds to the falling edge of the voltage pulse. As shown in Fig. 5, the EL transients recorded with this method display three distinct features in the temporal range observed: (1) a region where the EL intensity remains constant, in a time range lasting at least 1 μs after the voltage is removed; followed by (2) a region where the EL shows a transient EL spike over a temporal range of 1–10 μs; and finally (3) a region where the EL monotonically decays, which lasts up to a few ms after the voltage is switched-off.

In the literature, a model has been discussed to explain such transient EL behavior in small-molecule fluorescent OLEDs having a guest-host EML design.[24] According to this model, after the external voltage is switched off, preexisting excitons formed during the temporal region of steady-state operation or right after the voltage is switched-off for a period of time (here ca. 1 μs) and continue to sustain a similar EL amplitude than the one observed during steady-state operation. Meanwhile, longer-lived correlated charge pairs (CCPs) diffuse into each other to form excitons and radiatively recombine over time, generating a spike in the EL transient. Finally, as the CCP population decreases, the EL displays a tail which is attributed to the detrapping of long-lived trapped carriers, leading to the formation of CCPs and their radiative recombination. Assuming that the time-dependent luminance, $L(t)$, is directly proportional to the time-dependent density of singlet excitons (SEs), $N_{SE}(L_0, t)$,

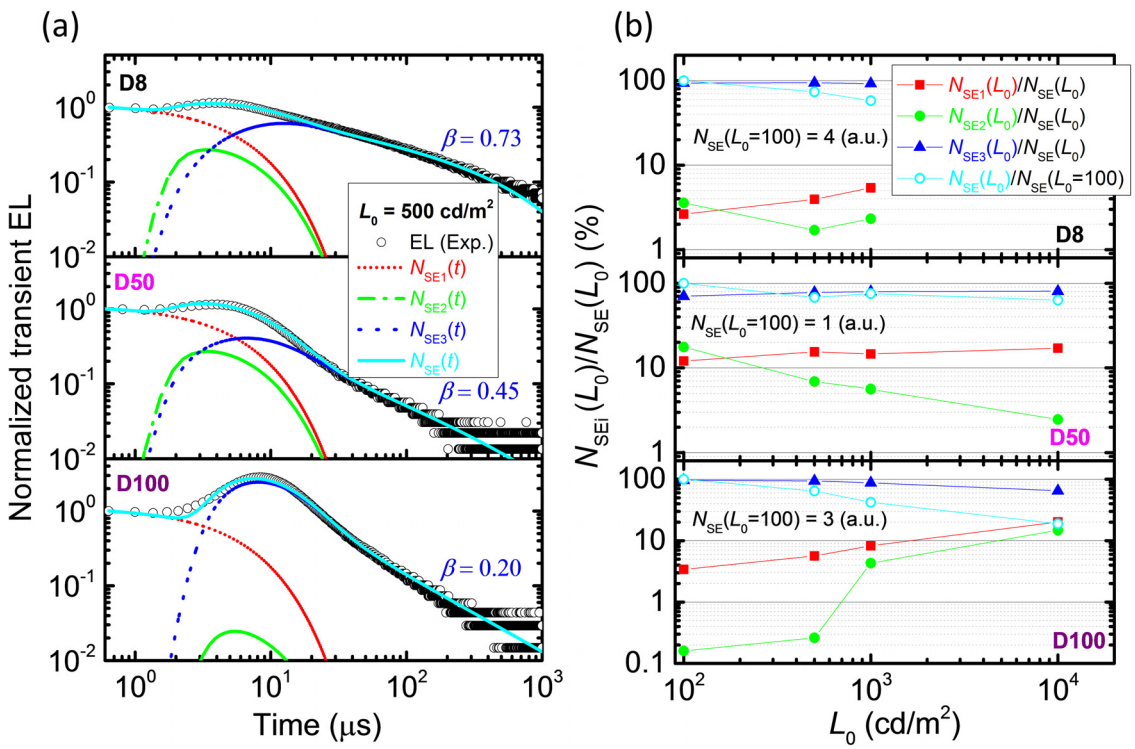

FIG. 5. (a) EL transients of D8, D50, and D100 normalized by their intensities at $L_0 = 500$ cd/m^2 and fitted by the CCP-model.[24] Experimental EL data (black circle), $N_{SE1}(t)$ (red, short dotted line), $N_{SE2}(t)$ (green, dashed-dotted line), $N_{SE3}(t)$ (blue, dotted line), and the total concentration $N_{SE}(t)$ (cyan, solid line) are displayed, respectively. (b) Under different L_0 values, the individual contribution of $N_{SEi}(L_0)$ to $N_{SE}(L_0)$ in D8, D50, and D100, respectively. Also, in each device, $N_{SE}(L_0)$ is normalized by $N_{SE}(L_0 = 100)$ as shown by cyan-circle symbols. $N_{SE}(L_0 = 100)$ of D8 and D100 are represented by the $N_{SE}(L_0 = 100)$ value of D50, which is normalized to a single unit.

this model suggests that the EL transient can be decomposed into three different processes

$$L(t) \propto N_{SE}(L_0, t) = N_{SE1}(L_0, t) + N_{SE2}(L_0, t) + N_{SE3}(L_0, t), \quad (1)$$

where $N_{SE1}(L_0, t)$ represents the time-dependent SE population formed during steady-state operation at an initial luminance L_0, and immediately after the voltage is switched off; $N_{SE2}(L_0, t)$ represents SEs that arise from the recombination of CCPs after the voltage pulse is switched off; and $N_{SE3}(L_0, t)$ represents SEs that arise from the recombination of CCPs generated from initially uncorrelated charge carriers that are slowly detrapped from deep traps in the EML. The model closely describes the transient EL signals measured on all devices and at all different initial luminance values (L_0), as shown in Fig. S4 of the supplementary material, and a detailed description of the model and fitting parameters can be found in Figs. S5–S7 of the supplementary material.

Figure 5(a) shows the results of fitting this model to the normalized EL transients measured in devices D8, D50, and D100, from an initial steady-state $L_0 = 500\,\text{cd/m}^2$. To rationalize the results derived from fitting the EL(t) data, we first calculated the total density of SEs observed through these experiments as well as the one attributed to each of the three different processes. These total densities are calculated by integrating the time-dependent distributions $N_{SEi}(L_0, t)$ ($i = 1, 2, 3$) over the time range from 0 to 1000 μs

$$N_{SE}(L_0) = \sum_{i=1,2,3} N_{SEi}(L_0) = \sum_{i=1,2,3} \int_0^{1000} N_{SEi}(L_0, t)dt. \quad (2)$$

Figure 5(b) shows the percentage that each of these processes contributes to the total density of SEs as a function of L_0 in D8, D50, and D100, respectively. This analysis reveals a clear difference between the behavior of the EL in D50 and that observed in other devices. First of all, it should be noted that for $L_0 < 10\,000\,\text{cd/m}^2$, D50 shows the smallest $N_{SE}(L_0)$. For instance, at a same initial $L_0 = 100\,\text{cd/m}^2$, D8 and D100, respectively, emit approximately 4 times and 3 times the light of D50 [when $N_{SE}(L_0 = 100)$ of D50 normalized as 1 unit as shown in Fig. 5(b)], after the voltage is switched off. A large EL output [i.e., a large total concentration of $N_{SE}(L_0)$] produced after the device is switched off is not desirable since it reveals the existence of physical mechanisms leading to inefficient charge recombination in the device. This trends holds when L_0 is increased up to 1000 cd/m^2, although this difference is reduced to 2.8 times the light of D50 (0.75 units) for D8 (2.1 units) and to 1.6 times for D100 (1.2 units). For $L_0 = 10\,000\,\text{cd/m}^2$, D100 (0.54 units) emits 0.85 times the light of D50 (0.63 units) after the voltage pulse is switched off; D8 devices do not reach this luminance value due to a very large EQE roll-off.

With these results in mind, we direct our attention to the individual contributions of $N_{SE}(L_0)$ and note that at $L_0 = 100\,\text{cd/m}^2$, D50 shows the largest concentration of $N_{SE1}(L_0)$ (12%) and $N_{SE2}(L_0)$ (18%), and the lowest of $N_{SE3}(L_0)$ (70%) when compared to those found in D8 and D100. A large concentration of $N_{SE1}(L_0)$ excitons can be attributed to efficient transport and recombination of carriers leading to the rapid formation of SEs right after the voltage is turned off. This is further supported by the large $N_{SE2}(L_0)$ concentration in D50, and the fact that the maximum of the EL peak created by CCPs occurs at an earlier time than those of D8 and D100 [see Fig. 5(a)], which indicates that a large concentration of free carriers are within the Onsager radius and quickly diffuse into each other to recombine radiatively. While in an ideal device it would be desirable to minimize $N_{SE}(L_0)$ in general, finding strategies to minimize $N_{SE3}(L_0)$ seems to be particularly important to improve efficiency, since $N_{SE3}(L_0)$ represents trapped or moving, unpaired electrons and holes, which remain for a long time in the EML without radiatively recombining and consequently lead to increased probability of non-radiative polaron-exciton recombination events.

Hence, at low luminance values, the larger EQE_{10} shown by D50 devices when compared with EQE values shown by D8 and D100 can be attributed to the more efficient formation of excitons and CCPs and to the lower concentration of trapped or slow-moving carriers. In this context, it is worth noting that in the model, the term $N_{SE3}(L_0)$ is described as the convolution of the rate of change in the concentration of carriers diffusing through an exponential trap distribution (described by the parameter β) with the CPP recombination rate [see Eq. (6) in the supplementary material]. As shown in Fig. 5(a), the value of β decreases from 0.73 in D8 to 0. 20 in D100, implying that trapped carriers will take much longer to recombine in D8 than in D100 and consequently creating long-lived EL tails. This behavior seems to support the assumption that, in D8, oBFCzTrz acts as a deep trap in the context of carrier transport, while in pristine oBFCzTrz EMLs, carriers will face narrower trap distributions. Hence, differences in $N_{SE3}(L_0)$ values between devices are related to differences in the uncorrelated electron and hole populations in the EML and/or to the existence of a recombination zone that is not homogenously distributed across the thickness of the EML. Either of these two situations will cause unpaired carriers to have to travel a longer distance before they form a CCP and consequently will increase the population of "trapped" carriers and the strength of the delayed EL. What seems perhaps remarkable from our results is that, despite the large energetic and positional disorder that could be expected from mixing DPEPO and oBFCzTrz at 1:1 vol. ratio, the population of trapped carriers in D50 is much smaller than those in D8 and D100.

III. CONCLUSION

We performed detailed studies of the effects on OLED performance of varying the oBFCzTrz concentration from 8 wt. % to 100 wt. % in a DPEPO host. We found that highly efficient OLEDs in which oBFCzTrz is doped at 50 wt. % in DPEPO can achieve EQE values up to 25.5% at 10 cd/m^2, along with small EQE roll-off values that allow them to yield an EQE of 22.8% at 1000 cd/m^2 and 16.4% at 10 000 cd/m^2. At these high oBFCzTrz concentrations, aggregation effects cause (1) a small reduction of the PLQY of the EML, from

100% displayed by an EML having an oBFCzTrz concentration of 8 wt. %, to 90% displayed by an EML having a oBFCzTrz concentration of 50 wt. %, and (2) a slight red shift of the PL and EL spectra. Despite these detrimental effects, the introduction of oBFCzTrz at a large weight ratio of up to 50 wt. % improves the recombination efficiency in the EML, leading to devices with an improved performance compared to devices having EMLs with lower concentrations of oBFCzTrz. Beyond an oBFCzTrz concentration of 50 wt. %, the devices continue to exhibit good performance characteristics with decreasing maximum EQE values but also with decreased EQE roll-off-values. OLEDs having an EML comprised of a pristine oBFCzTrz layer yield a maximum EQE of 14.0% with a small EQE roll-off of 10% up to a luminance of 5400 cd/m^2. Single carrier devices and transient EL studies have been used to investigate charge transport, recombination, and the EL dynamics in these devices and provide useful insights into the behavior of devices presented in this study and should contribute to device optimization strategies.

SUPPLEMENTARY MATERIAL

See supplementary material for additional information.

ACKNOWLEDGMENTS

This material is based in part upon the work supported by the U.S. Department of Energy's Office of Energy Efficiency and Renewable Energy (EERE) under the Solid-State Lighting Program Award No. De-EE0008205. This work was supported in part through a grant from the Mitsubishi Chemical Corporation.

[1]M. A. Baldo *et al.*, Nature **395**, 151–154 (1998).
[2]K. Udagawa, H. Sasabe, C. Cai, and J. Kido, Adv. Mater. **26**, 5062–5066 (2014).
[3]Q. Wang *et al.*, Adv. Mater. **26**, 8107–8113 (2014).
[4]M. Y. Wong and E. Zysman-Colman, Adv. Mater. **29**, 1605444 (2017).
[5]T. Lin *et al.*, Adv. Mater. **28**, 6976–6983 (2016).
[6]D. R. Lee *et al.*, ACS Appl. Mater. Interfaces **7**, 9625–9629 (2015).
[7]W. Zeng *et al.*, Adv. Mater. **30**, 1704961 (2018).
[8]C. Murawski, K. Leo, and M. C. Gather, Adv. Mater. **25**, 6801–6827 (2013).
[9]N. C. Giebink *et al.*, J. Appl. Phys. **103**, 044509 (2008).
[10]N. C. Giebink and S. R. Forrest, Phys. Rev. B **77**, 235215 (2008).
[11]K. Sato *et al.*, Phys. Rev. Lett. **110**, 247401 (2013).
[12]Q. S. Zhang *et al.*, Adv. Mater. **27**, 2096–2100 (2015).
[13]B. S. Kim and J. Y. Lee, Adv. Funct. Mater. **24**, 3970–3977 (2014).
[14]J. W. Sun *et al.*, Adv. Mater. **26**, 5684–5688 (2014).
[15]D. R. Lee *et al.*, ACS Appl. Mater. Interfaces **8**, 23190–23196 (2016).
[16]W. L. Tsai *et al.*, Chem. Commun. **51**, 13662–13665 (2015).
[17]J. J. Guo *et al.*, Adv. Funct. Mater. **27**, 1606458 (2017).
[18]Y. Wada *et al.*, Appl. Phys. Express **9**, 032102 (2016).
[19]J. Lee, N. Aizawa, M. Numata, C. Adachi, and T. Yasuda, Adv. Mater. **29**, 1604856 (2017).
[20]H. S. Kim, S. R. Park, and M. C. Suh, J. Phys. Chem. C **121**, 13986–13997 (2017).
[21]C. A. Zuniga *et al.*, Adv. Mater. **25**, 1739–1744 (2013).
[22]S. Gong *et al.*, Chem. Mater. **26**, 1463–1470 (2014).
[23]P. L. dos Santos, F. B. Dias, and A. P. Monkman, J. Phys. Chem. C **120**, 18259–18267 (2016).
[24]R. Liu, Z. Gan, R. Shinar, and J. Shinar, Phys. Rev. B **83**, 245302 (2011).
[25]A. Salehi, Adv. Opt. Mater. **5**, 1700197 (2017).